ELSEVIER

Thermochimica Acta 386 (2002) 161–172

thermochimica acta

www.elsevier.com/locate/tca

Effect of thermal treatments on catalyst reducibility and activity in nickel supported on RHA–Al_2O_3 systems

Feg-Wen Chang*, Ming-Tseh Tsay, Maw-Suey Kuo

Department of Chemical Engineering, National Central University, Chungli 32054, Taiwan

Received 12 June 2001; received in revised form 5 September 2001; accepted 25 September 2001

Abstract

RHA–Al_2O_3 composite oxide supports were prepared by impregnation of rice husk ash with an aluminum sulfate solution, and were then used to prepare Ni/RHA–Al_2O_3 catalysts by the ion exchange method. The supports and catalyst precursors were characterized by X-ray diffraction (XRD) and transmission electron microscopy (TEM). The thermal decomposition of catalyst precursors was examined by a thermogravimetric analyzer (TGA). In addition, the effect of calcination temperature on the catalyst reducibility was investigated by the temperature-programmed reduction (TPR) technique. Results show that the decomposition temperature of layered nickel compound to nickel oxide started above 773 K. Reduction in NiO from the thermal decomposition of the layered nickel compound was found to be particularly difficult. The reduction temperature increased with the increase in calcination temperature. The catalytic activities of nickel catalysts were tested by CO_2 hydrogenation with H_2/CO_2 ratios of 4/1 at 773 K. The effects of calcination temperature, calcination time, reduction temperature, reduction time and alumina content on the activity of catalysts were examined extensively. An optimal condition for calcination and reduction of catalysts has been determined from activity considerations in the hydrogenation of CO_2.

Keywords: Ni/RHA–Al_2O_3 catalyst; Catalyst reducibility and activity; CO_2 hydrogenation; Thermal treatment; Ion exchange

1. Introduction

Nickel supported on silica, alumina, or silica–alumina materials are used in many industrial catalytic processes such as hydrogenation [1–6], hydrogenolysis [7–9], and steam-reforming [10], due to its easy availability, high activity, and low cost. The chemical and physical structure of nickel supported on silica and alumina has been the subject of many investigations. Yet there is little information on silica–alumina-supported nickel catalysts. Supported metal catalysts are often prepared by incipient wetness impregnation, deposition–precipitation and ion exchange techniques with different precipitating agents, followed by a suitable thermal activation procedure corresponding to calcination and/or reduction steps. The characteristic and distribution of surface nickel compounds on the support depend on the preparation procedure and the activation conditions of the different precursors. This results in different extents of what is called 'interaction' between nickel and support, thus influencing the general performance of the catalyst. Therefore, the activation procedure, i.e. the calcination and the reduction, is of vital importance, and researchers become particularly interested in its study.

* Corresponding author. Tel.: +886-3-4227151x4202; fax: +886-3-4252296.
E-mail address: fwchang@cc.ncu.edu.tw (F.-W. Chang).

0040-6031/02/$ – see front matter
PII: S0040-6031(01)00771-7

Burch [7] and Burch and Flambard [8], Aguinaga et al. [11] and other researchers [9,12–16] have studied nickel/silica–alumina catalysts using different techniques. Although most of the results obtained are very interesting, these researchers have restricted their work to impregnation or precipitation–deposition method. Moreover, most of them have focused on specific aspects in the catalyst activity or characteristics, but they seldom combine the results systematically to obtain an overall picture of the catalysts. This is important from the point of view of applied catalysis.

Rice husk is a major waste product of the agriculture industry. The major constituents of rice husk are cellulose, lignin and ash. Amorphous silica (commonly referred to as rice husk ash (RHA)) with a high specific surface area, high melting point and porosity, was extracted from rice husk by acid leaching, pyrolysis, and carbon-removing processes [17,18]. In our previous reports [19–22], we have found that the RHA-supported nickel catalyst used for hydrogenation of CO_2 exhibited higher activity than those prepared by silica gel. In the present investigation, the RHA was used as raw material to prepare silica–alumina composite oxide supports. Nickel catalysts supported on various composite oxides were prepared with about 4.0 wt.% nickel loading using the ion exchange method. The reducibility of Ni/RHA–Al_2O_3 catalysts was investigated using temperature-programmed reduction (TPR) technique and by hydrogenation of CO_2 the catalytic activity of these catalysts has been assessed. To examine how preparation and activation conditions influence the activity of catalysts, the effects of calcination temperature, calcination time, reduction temperature, reduction time and alumina content during catalyst preparation were investigated.

2. Experimental

2.1. Raw material

The raw material was rice husk obtained from a rice mill. The rice husk was washed thoroughly with distilled water to remove adhering soil and was then dried at 373 K in an air oven. The processes of acid leaching, pyrolysis, and carbon-removing were carried out as detailed in our previous reports [17–22]. The dried rice husk was refluxed with 3N HCl solution in a round-bottomed glass flask at 373 K within a thermostat for 1 h. After leaching, the husk was washed repeatedly with distilled water until the filtrate was free from acid, and then dried. The pyrolysis process was performed in a tubular quartz reactor under a nitrogen atmosphere at 1173 K for 1 h. After pyrolysis, the husk was further heated in an air furnace at 1173 K for 1 h; and the husk, thus obtained contained more than 99% amorphous silica. This silica was then used as raw material to prepare silica–alumina composite oxide supports.

Aluminum sulfate (Merck, 99%) was used to prepare the composite oxide supports. Nickel nitrate (Merck, 99%) and aqueous ammonia (Merck, 25%) were used to prepare the catalysts.

2.2. Sample preparation

Silica–alumina composite oxide supports were prepared according to the method described by Aguinaga et al. [11]: the RHA was impregnated with an aqueous solution of aluminum sulfate in proportions adjusted to obtain different content of alumina in the silica–alumina. After impregnation, the samples were dried at 393 K for 24 h and calcined in air at 1123 K for 2 h. We named this silica–alumina composite oxide supports system as RHA–Al_2O_3.

Nickel catalysts supported on the RHA–Al_2O_3 composite oxides were prepared by ion exchange. An aqueous solution of nickel nitrate was brought to a desired pH value by the addition of concentrated ammonia before supports were added. The concentration of nickel nitrate was adjusted to yield catalysts of about 4.0 wt.% loading [21]. The suspensions were kept at 298 K in a thermostat vessel and stirred for 24 h to reach the thermodynamic equilibrium of adsorption [23]. The pH value was maintained at 8.5 during the exchange of nickel complex cation with hydroxyl protons on the surface of the support by the addition of dilute ammonia [21]. When the process was completed, the solid was washed with distilled water and filtered, the final filter cake was dried in an air oven and were further calcined in a furnace. Finally, the catalyst precursors were activated by placing the samples in the TPR apparatus to be reduced. The effects of different variables at each

Table 1
Al_2O_3 content and nickel loading of various catalysts.

Catalyst type	Al_2O_3 content (wt.%)	Nickel loading (wt.%)
Ni/RHA–Al_2O_3-1	1.69	3.84
Ni/RHA–Al_2O_3-2	5.17	4.10
Ni/RHA–Al_2O_3-3	9.80	3.74
Ni/RHA–Al_2O_3-4	14.71	4.44
Ni/RHA–Al_2O_3-5	18.70	4.38

stage on the resulting catalyst are discussed later in this paper.

2.3. Characterization

The actual nickel loading of the catalyst and alumina content of the supports determined by inductively coupled plasma-atomic emission spectrometer (ICP-AES) were shown in Table 1.

The specific surface area, average pore diameter and pore volume of sample were obtained in an ASAP 2000 apparatus from nitrogen adsorption at 77.35 K after degassing at 473 K.

The acidity of the RHA–Al_2O_3 and RHA were determined by *n*-butylamine temperature-programmed desorption (*n*-$C_4H_9NH_2$-TPD) [15] using a conventional flow system with flame ionization detector. For each run, about 30 mg of the sample was loaded into a U-type quartz reactor and dehydrated at 673 K for 2 h with sufficient nitrogen. Then, the reactor was cooled down to room temperature and the saturated gas of *n*-butylamine was passed down, flowing through the bed for 30 min. After *n*-butylamine adsorption, samples were purged in the carrier flow at 423 K in order to remove physisorption. Finally, the desorption step was performed from 423 to 873 K at a heating rate of 10 K/min and a helium flow of 30 ml/min.

X-ray powder diffraction patterns of the catalyst precursors as well as RHA–Al_2O_3 were obtained by a X-ray diffractometer using Cu Kα radiation with a wavelength of 1.5406 Å, from 5 to 80° at a rate of 0.05°/s.

TPR mesaurements were carried out on about 50 mg of catalysts precursors which were placed in the quartz reactor in a tubular furnace and heated from room temperature to 1273 K at 10 K/min under a 40 ml/min H_2/Ar (5/95) flow stream. The hydrogen consumption as a function of temperature was detected by a thermal conductivity detector (TCD) which was monitored by a computer.

Transmission electron microscopy (TEM) studies were performed on a JEOL JEM-2000FX II instrument operated at 160 kV. The sample was suspended in *n*-butyl alcohol and ultrasonically dispersed for 20 min. The suspension was then pipetted onto a copper microgrid with carbon film [24].

The thermogravimetric analysis of the samples was carried out in a Perkin- Elmer TGA7 thermobalance, in an air flow and heating rate at 10 K/min, to determine the loss of weight that takes place during the decomposition process.

2.4. Hydrogenation of CO_2

The activity of nickel catalysts in CO_2 hydrogenation has been evaluated at 773 K for 4 h operating at atmospheric pressure. The experimental setup has been described previously [19,20]. For each run, about 50 mg of catalysts were loaded into a quartz reactor of 0.25 in. i.d. and reduced in situ under a continuous flow of H_2/Ar (5/95) at the rate of 40 ml/min. After reduction, the reactor was adjusted to the temperature of 773 K under the same hydrogenation flow. As the temperature became stabilized, the flow rates of carrier gas He and a H_2/CO_2 (4/1) mixture were adjusted to 30 and 25 ml/min, respectively, and fed into the reaction system. All reactant and product gas concentrations were analyzed by gas chromatograph with a TCD.

3. Results and discussion

Table 2 shows the BET surface area, total pore volume and average pore diameter of the calcined RHA–Al_2O_3 composite oxide supports. Bare RHA is also listed for comparison. The impregnation of alumina on RHA resulted in a decrease in the surface area of RHA. The BET surface area of the composite oxides after calcination was gradually decreased with alumina content up to 9.8 wt.% and then increased further. These findings can be explained by the mechanism of aluminum phase formation during preparation. At low alumina content, the alumina blocked

Table 2
Characteristics of RHA and RHA–Al_2O_3 composite oxide supports

Support type	BET surface area (m^2/g)	Total pore volume (cm^3/g)[a]	Average pore diameter (Å)[b]	Acidity (μmol/g)[c]
RHA	157	0.28	57	0
RHA–Al_2O_3-1	146	0.25	58	39.9
RHA–Al_2O_3-2	131	0.20	52	77.2
RHA–Al_2O_3-3	127	0.18	46	90.4
RHA–Al_2O_3-4	129	0.24	59	108.4
RHA–Al_2O_3-5	137	0.33	78	102.2

[a] N_2 adsorption method.
[b] BJH desorption average pore diameter.
[c] Measured by $C_4H_9NH_2$-TPD.

the micropores of RHA and reduced the surface area, which then resulted in a small pore volume. At high alumina content, the presence of a sufficiently porous surface compound of aluminum means that many macropores were produced during calcination; these phenomena led to a large pore volume and an increase in surface area.

We have examined here the dependence of acidity on alumina content of composite oxide supports; the result is also presented in Table 2. The total acidity of the composite oxide supports increased with alumina content up to a certain value and remained almost unchanged. This may be explained by the mechanism of alumina plating. At low alumina content, the RHA remained partly naked, inferring that the Bronsted-type acid was produced at the interface of the RHA and alumina. Moreover, the Lewis-type acid concentrated on the surface of alumina particles [25,26]. Consequently, an increase in alumina content implied an increase in total acidity of supports. Up to a certain alumina content, almost the whole RHA was coated with alumina particles. Only the Lewis-type acid concentrated on the surface of the composite oxide supports, and therefore, the acidity remained unchanged with further increase in alumina content.

Fig. 1 shows the XRD pattern of the RHA, calcined RHA–Al_2O_3 composite oxide supports and Ni/RHA–Al_2O_3-4 catalyst precursors. X-ray diffractograms of the RHA, as shown in Fig. 1a, reveal the broad background peak associated with the amorphous nature of silica. Fig. 1b–d show the XRD patterns of the different composite oxide support with 1.69, 5.17 and 9.8 wt.% alumina content, respectively. It can be seen that no detectable peak appeared for alumina, indicating a homogenous dispersion of small crystallites of alumina over RHA at lower alumina content. This phenomenon is similar to that previously reported by Kumbhar [27]. At higher alumina content, they display small and broad traces as shown in spectra (Fig. 1e and f). These peaks correspond to γ-phases of alumina, which are amorphous in nature. The intensity of broad background peak (at $2\theta = 22^\circ$) decreases slightly as the alumina content increases (Fig. 1b–f). This may be due to the complete coating

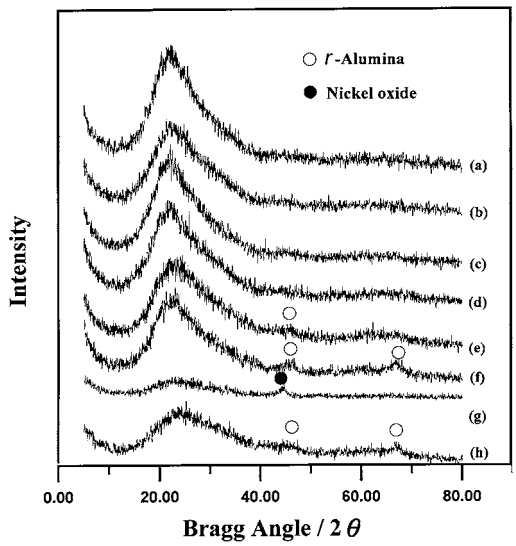

Fig. 1. XRD spectra of raw materials, composite oxide supports and catalyst precursors. (a) Rice husk ash; (b) RHA–Al_2O_3-1; (c) RHA–Al_2O_3-2; (d) RHA–Al_2O_3-3; (e) RHA–Al_2O_3-4; (f) RHA–Al_2O_3-5; (g) Ni/RHA–Al_2O_3-4 after calcination at 773 K; (h) unsupported aluminum sulfate quenched at TGA examination.

of the RHA with alumina at higher alumina content. In Fig. 1g, the XRD pattern of the Ni/RHA–Al_2O_3-4 catalyst precursor after calcination at 773 K displays one small and broad peak corresponding to nickel oxide that appears less well-crystallized. In addition, the bare alumina obtained from unsupported alumium sulfate quenched at TGA examination is also shown in Fig. 1h for comparison. Fig. 1h shows that the γ-alumina was amorphous in nature.

To understand the chemical changes during calcination, the thermal decomposition of unsupported aluminum sulfate($Al_2(SO_4)_3{\cdot}18H_2O$), supported aluminum sulfate (RHA–Al_2O_3-4 precursor) and catalyst precursors (Ni/RHA–Al_2O_3-2 and Ni/RHA–Al_2O_3-4) after the drying step are examined by a thermogravimetric analyzer (TGA). The weight change and the derivatives versus temperature diagrams are shown in Fig. 2. Fig. 2a reveals that the decomposition of unsupported aluminum sulfate to alumina completed above 1198 K (XRD analysis shown in Fig. 1h confirms the formation of γ-alumina). An initial weight loss is observed between 393 and 493 K, and may be attributed to the desorption of water. The weight loss of aluminum sulfate changes drastically at the final step. This weight losses may be attributed to the decomposition of $Al_2(SO_4)_3$, i.e. $Al_2(SO_4)_3$ into γ-Al_2O_3. Fig. 2b shows the corresponding TGA for supported aluminum sulfate. It is interesting to note that the final maximum temperature of the supported aluminum sulfate (1101 K) is lower than that of the unsupported aluminum sulfate (1162 K). The rate enhancement by the support could be due to an increase in lattice defects and nucleation site densities in the small blocks of Al(III) on the surface. However, it is also possible that the enhancement arises from reaction of the RHA surface with aluminum sulfate, probably via surface OH groups, to form surface aluminosilicate [28]. Fig. 2c and d show the TGA traces for the Ni/RHA–Al_2O_3-2 and Ni/RHA–Al_2O_3-4 catalyst precursors after the drying step, respectively. As can be seen, the decomposition temperature of nickel compound to nickel oxide started above 773 K. XRD result shown in Fig. 1g also supports this point. Moreover, an initial weight loss is observed between 308 and 393 K, which is associated with the hydration of the adsorbed complex. This peak was used to determine the minimum temperature of the drying step.

The TEM of the RHA–Al_2O_3-4 composite oxide supports and the Ni/RHA–Al_2O_3-4 catalyst precursors are presented in Fig. 3. Fig. 3b shows the surface structure of the Ni/RHA–Al_2O_3-4 catalysts after drying (without prior calcination). The foil-like structures distributed over the support with random orientations are not present on the RHA–Al_2O_3-4 (Fig. 3a) before ion exchange and are of size larger than 5 nm in width. These structures may be attributed to nickel aluminates according to previous reports [16,29–32]. These nickel aluminates can be described as a superimposition of sheets composed of several layers.

TPR was used to characterize the catalyst precursor with respect to the degree of interaction with support and nickel, by monitoring the variation in the calcination stages of catalyst preparation. The TPR profiles of Ni/RHA–Al_2O_3-4 catalyst precursors calcined at 573, 773, 973 and 1173 K are shown in Fig. 4. The profiles of the sample calcined at 573 K exhibit a very broad reduction peak. A layered nickel compound formed can be observed in TEM results (Fig. 3b). The thermal decomposition of the layered nickel compound starts above 773 K according to the results of TGA (Fig. 2d). Consequently, the NiO phase is not present in the samples calcined at 573 K and layered nickel compound appears to be the main nickel species present. Therefore, the peak can be attributed to the reduction of layered nickel compound. When the calcination temperature increases, catalysts become less reducible. When the calcination temperatures reach 1173 K, the reduction extends to very high temperature. Although the main NiO present in the sample was confirmed by XRD results (Fig. 1g), the reducibility of this NiO phase seems to be strongly hindered when compared with that of the unsupported NiO. Such results are also found in earlier reports [21,29,33]. The reduction in nickel oxide resulting from the decomposition of the layered nickel compound is particularly difficult. It could be due to the presence of alumina trapped in the NiO particles as a result of increase in activation energy of reduction [32]. It is likely that the thermal decomposition of layered nickel compound does not yield pure nickel oxide; instead, alumina impurities may be present in the NiO lattice. Undoubtedly, this assumption can be confirmed in the view of a less well-crystallized state of the NiO as shown by XRD (Fig. 1g). Consequently, the less reducible NiO has been attributed to the interaction between the NiO

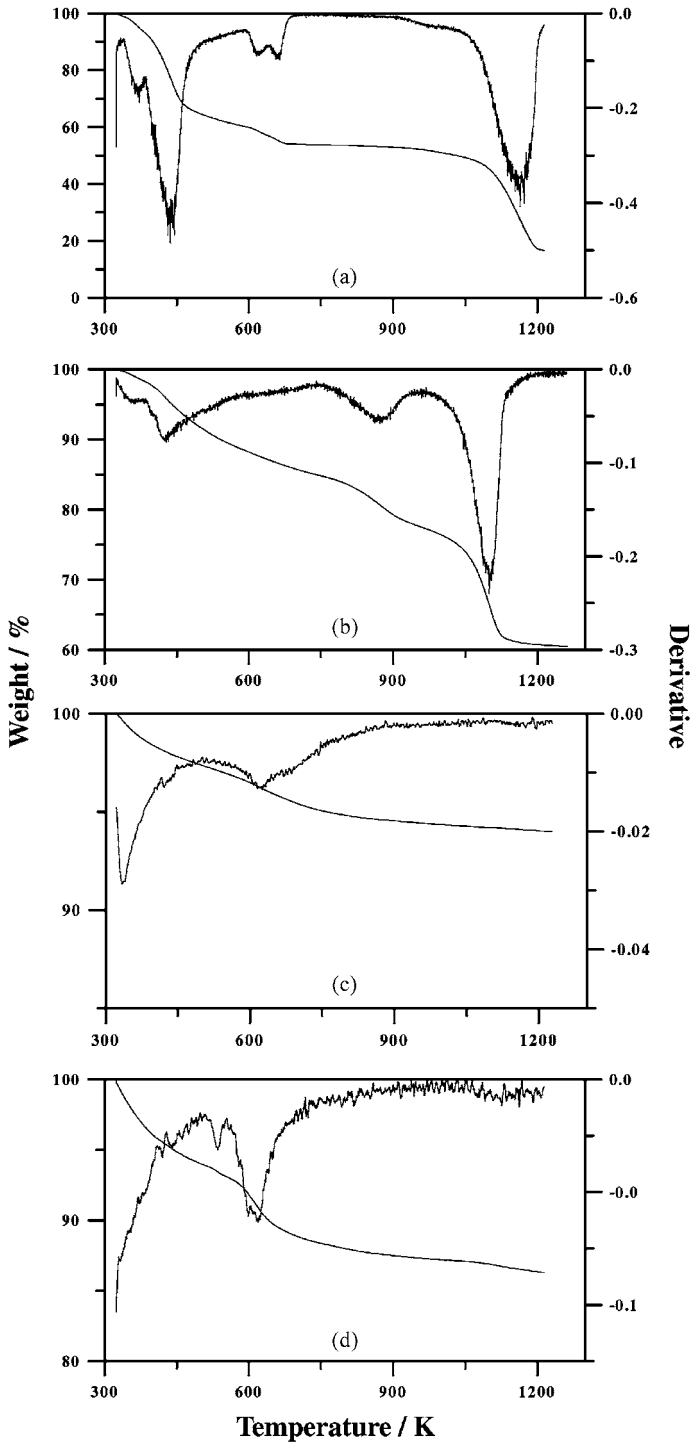

Fig. 2. Curves of TGA. (a) Unsupported aluminum sulfate; (b) aluminum sulfate supported on RHA after drying; (c) Ni/RHA–Al_2O_3-2 catalyst precursors after drying; (d) Ni/RHA–Al_2O_3-4 catalyst precursors after drying.

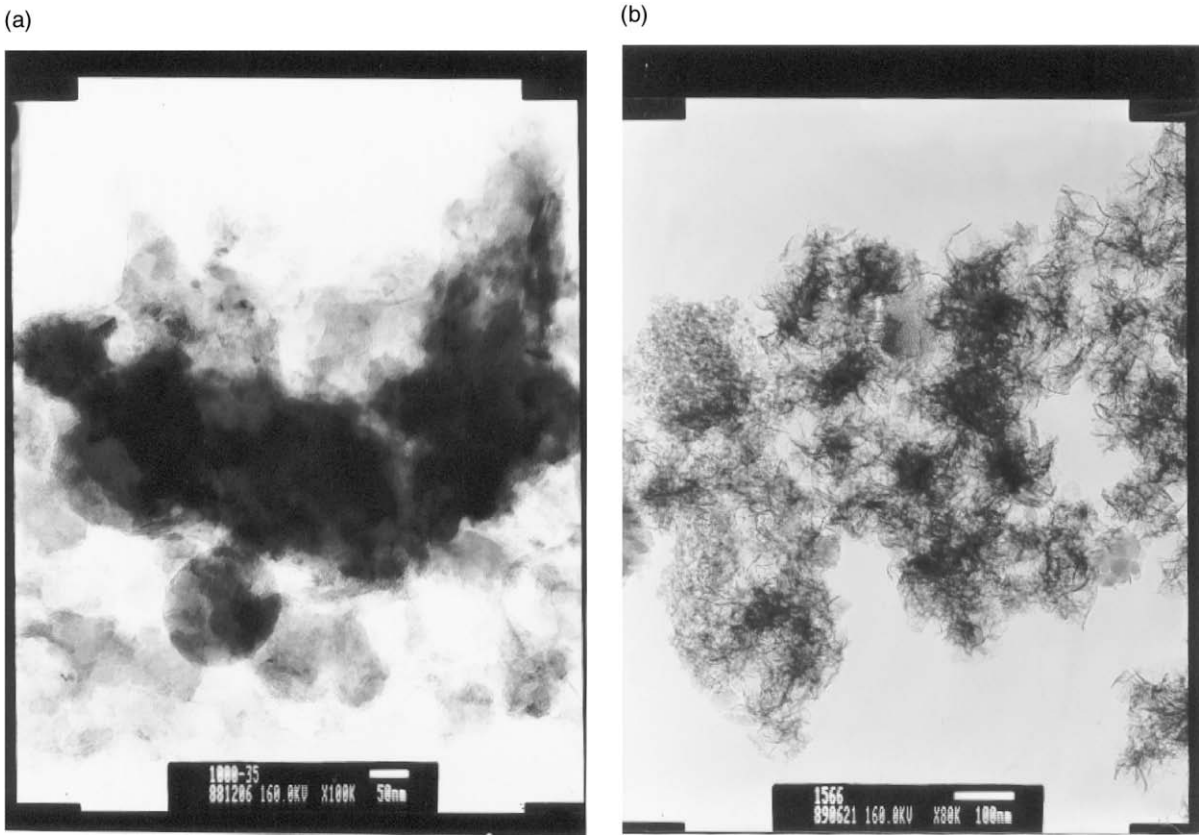

Fig. 3. Transmission electron micrograph of specimen. (a) RHA–Al_2O_3-4 composite oxide supports ($\times 100k$); (b) Ni/RHA–Al_2O_3-4 after drying ($\times 80k$).

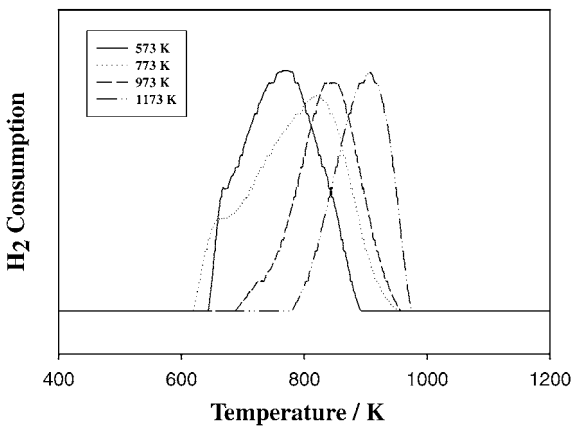

Fig. 4. TPR profiles of Ni/RHA–Al_2O_3-4 catalysts at different calcination temperatures for 4 h (ramp rate, 10 K/min).

and alumina following the decomposition of the layered nickel compound, as shown in Fig. 4. The higher the calcination temperature of the catalyst, the stronger the interaction between the NiO and alumina, and the more difficult it is for NiO to be reduced.

The calcination of catalyst precursor to metal oxide is a complex multistep solid-phase reaction, and many of these steps could be affected by the changes in nucleation rate, and the rate of metal oxide crystal growth of the support. Calcination of the precursors is carried out by thermal decomposition in air. The purpose of calcination is to eliminate the volatile and unstable anions and cations that are not desired in the final catalyst. In addition, a substantially elevated temperature is usually needed to increase the strength of the final catalysts. However, an excessive calcination temperature and longer calcination time

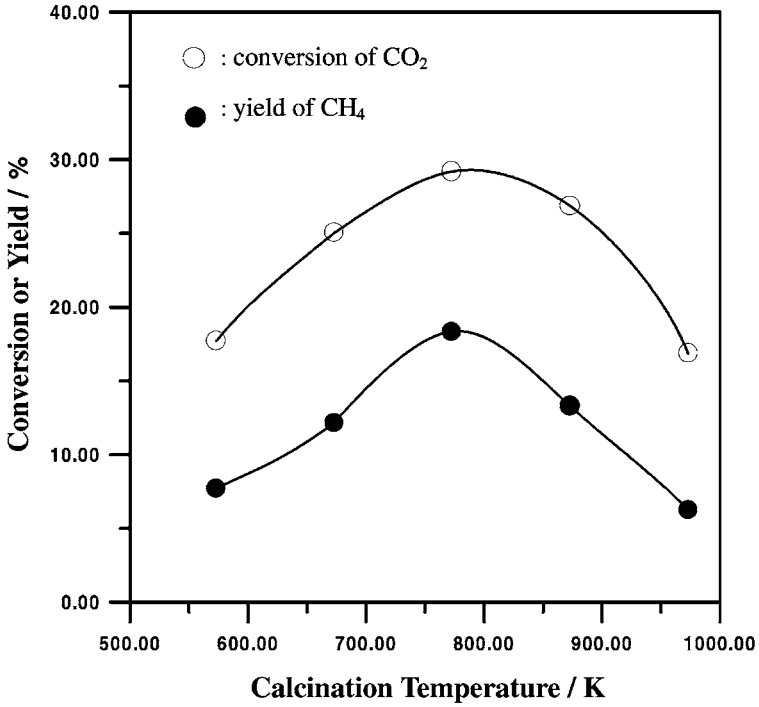

Fig. 5. Effect of calcination temperature on conversion and yield of CO_2 hydrogenation over Ni/RHA–Al_2O_3-4 catalysts (calcination time, 4 h; reduction temperature, 773 K; reduction time, 1 h).

will enlarge the size of the metal crystallites on the support and thus decrease the activity of the catalyst. Therefore, calcination under a suitable temperature will promote the activity of catalysts. Figs. 5 and 6 depict the effects of calcination temperature and calcination time on catalytic behavior of Ni/RHA–SiO_2-4 for hydrogenation of CO_2, respectively. Fig. 5 reveals that both the CO_2 conversion and CH_4 yield increased as the calcination temperature increased up to a maximum (773 K) and then decreased. Fig. 6 indicates that both the CO_2 conversion and CH_4 yield increased with increasing calcination time until 4 h and then decreased. This is because nickel oxide particles coalesce giving rise to large particles at higher calcination temperature and longer calcination time, followed by decreased activity. However, as shown in Fig. 4, it was hard to reduce the Ni/RHA–Al_2O_3-4 catalysts at higher calcination temperature, which then resulted in the decrease in active surface area. Venezia et al. [34] have studied the activity of pumice(aluminosilicate)-supported nickel catalysts for the hydrogenation of CO. From the experimental results, they also found that higher calcination temperatures have negative effects on activity of catalysts. Obviously, the calcination temperature of 773 K and calcination time of 4 h are the optimum conditions for the preparation of Ni/RHA–Al_2O_3-4 catalysts.

Figs. 7 and 8 present the effects of reduction temperature and reduction time on the catalytic behavior of Ni/RHA–Al_2O_3-4 for the hydrogenation of CO_2, respectively. The CO_2 conversion and CH_4 yield as a function of the reduction temperature are shown in Fig. 7. As can be seen, both conversion and yield increased with increasing reduction temperature up to 773 K, while with further increase in reduction temperature, the activity decreased. Fig. 8 reveals that the conversion of CO_2 and yield of CH_4 were independent of reduction time. Fig. 7 indicates that the activity of the catalyst increased with increasing reduction temperature at lower reduction temperature, due to an increasing amount of metallic nickel, as shown in the TPR patterns (Fig. 4). Proceeding with the reduction at too high a temperature results in a decrease in activity. That is probably due to the sintering at higher

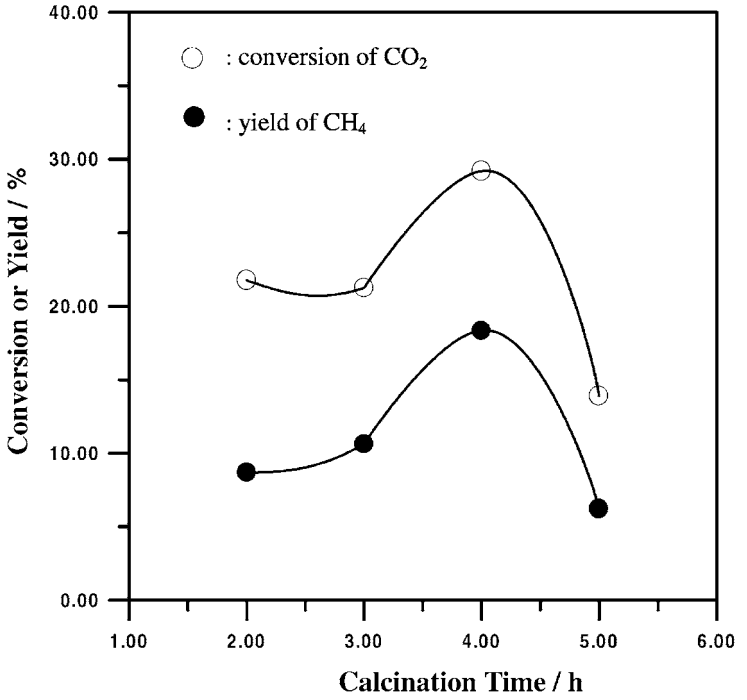

Fig. 6. Effect of calcination time on conversion and yield of CO_2 hydrogenation over Ni/RHA–Al_2O_3-4 catalysts (calcination temperature, 773 K; reduction temperature, 773 K; reduction time, 1 h).

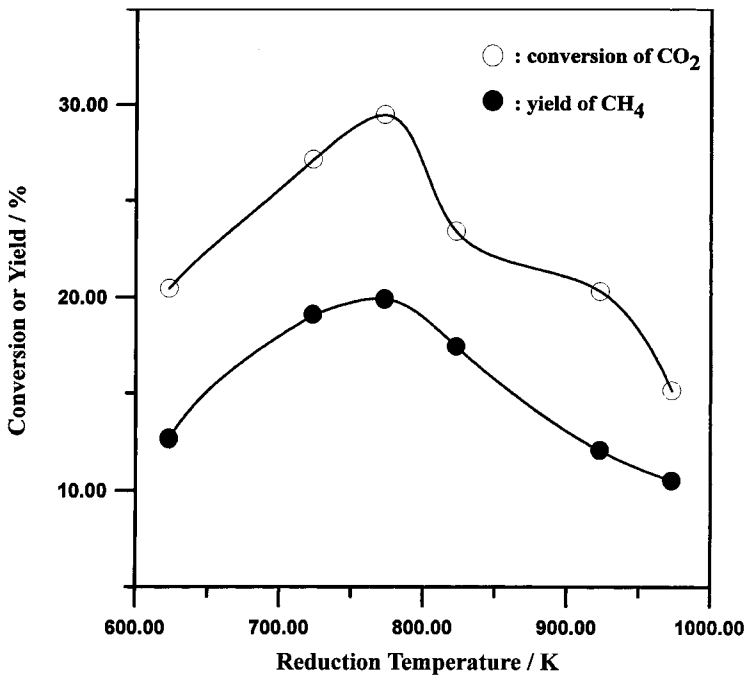

Fig. 7. Effect of reduction temperature on conversion and yield of CO_2 hydrogenation over Ni/RHA–Al_2O_3-4 catalysts (calcination temperature, 773 K; calcination time, 4 h; reduction time, 1 h).

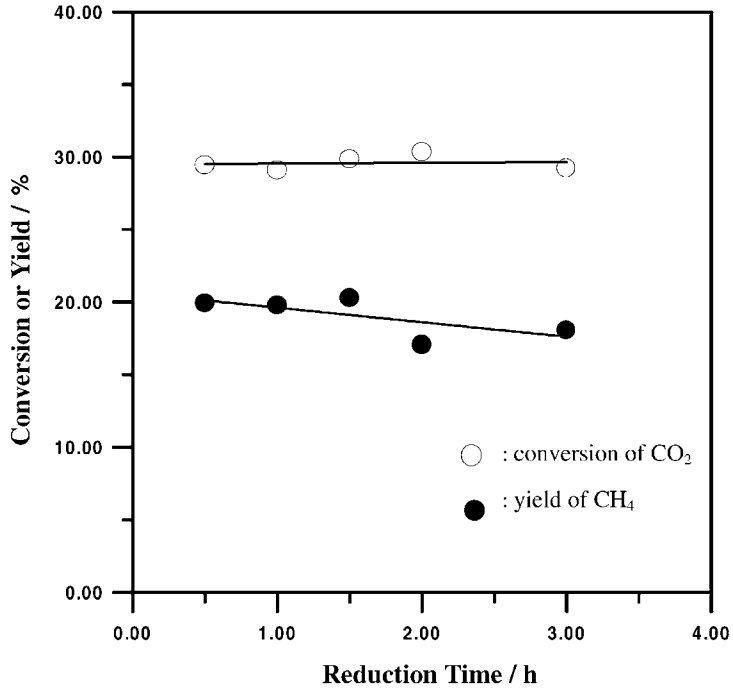

Fig. 8. Effect of reduction time on conversion and yield of CO_2 hydrogenation over Ni/RHA–Al_2O_3-4 catalysts (calcination temperature, 773 K; calcination time, 4 h; reduction temperature, 773 K).

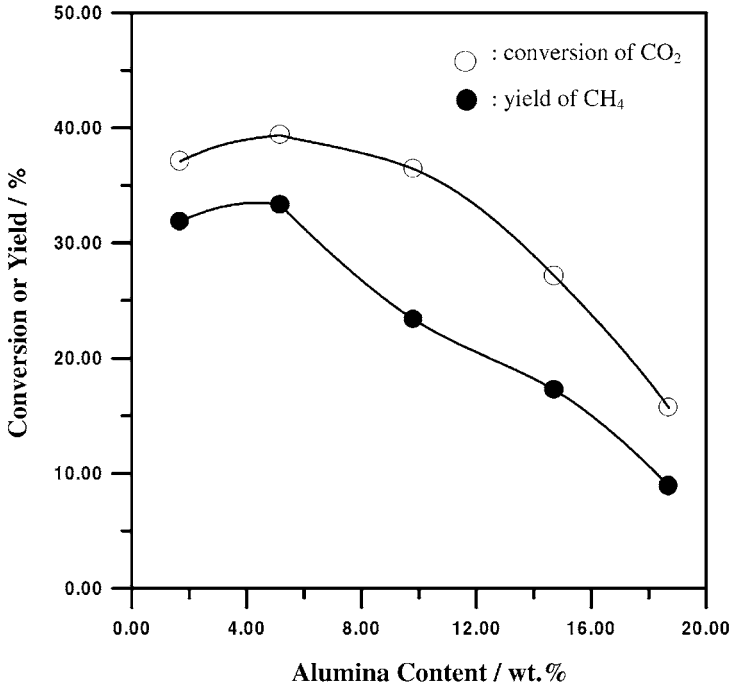

Fig. 9. Effect of alumina content on conversion and yield of CO_2 hydrogenation over nickel catalysts (calcination temperature, 773 K; calcination time, 4 h; reduction temperature,773 K; reduction time 1 h).

reduction temperature, which decreases the surface area of nickel. Loosdrecht et al. [35] investigated the catalytic hydrogenation of CO over Ni/SiO_2 catalysts prepared by impregnation method. They also found that the activity of Ni/SiO_2 catalysts is influenced by the reduction temperature.

Composite oxides of silica and alumina allow us to study systematically the effect of support acidity on the performance of supported metal catalysts. Fig. 9 displays the effects of alumina content on catalytic behavior of nickel catalyst supported on composite oxides for hydrogenation of CO_2. During this experiment, it has to be noted that the specific surface areas, pore sizes and surface properties of these five types of composite oxide supports are different as shown in Table 2. Consequently, it is difficult to control the nickel loading during the preparation of these catalysts by means of ion-exchange. However, the same preparation procedure was used giving about 4.0 wt.% nickel catalyst loading as presented in Table 1. As the figure reveals, CO_2 conversion and CH_4 yield decreased rapidly with increase in alumina content. The variations in the conversion of CO_2 and the yield of CH_4 are opposite to the changes in the amount of acid per catalyst supports as shown in Table 2. Consequently, a greater amount of acid per catalyst support implies a lower CO_2 conversion as well as CH_4 yield. We believe that the acidity of supports inhibits catalytic activity of CO_2 hydrogenation.

4. Conclusions

In this study, we used RHA as raw material to prepare five silica–alumina composite oxide supports, and then used these supports to prepare nickel catalysts by the ion exchange method. According to the results of *n*-butylamine chemisorption data, we found that acidity increased with alumina content up to a certain value, further increase in alumina content could not markedly increase the acidity. The thermal decomposition of the nickel compound with a layer structure starting above 773 K was determined by TGA. Reduction in NiO from the thermal decomposition of the layered nickel compound is found to be particularly difficult. The conversion of CO_2 and the yield of CH_4 are strongly dependent on the calcination and reduction temperatures. According to our findings, the optimal calcination and reduction temperatures are both 773 K for the $Ni/RHA–Al_2O_3$-4 catalysts. The hydrogenation activity decreases as alumina content increases. This indicates that acidity will not promote the hydrogenation of CO_2.

Acknowledgements

The authors express thanks to the National Science Council of Taiwan for its financial support under Project no. NSC 89-2214-E008-021.

References

[1] M.A. Vannice, J. Catal. 40 (1975) 129.
[2] M.A. Vannice, J. Catal. 44 (1976) 152.
[3] G.D. Weatherbee, C.H. Bartholomew, J. Catal. 68 (1981) 67.
[4] P.W. Yesgar, M. Sheintuch, J. Catal. 127 (1991) 576.
[5] L.P. Lindfors, T. Salmi, Ind. Eng. Chem. Res. 32 (1993) 34.
[6] J.A. Anderson, L. Daza, D.S. Damyanova, J.L.G. Fierro, M.T. Rodrigo, Appl. Catal. A 113 (1994) 75.
[7] R. Burch, J. Catal. 58 (1979) 220.
[8] R. Burch, A.R. Flambard, J. Catal. 85 (1984) 16.
[9] W.F. Taylor, D.J.C. Yates, J.H. Sinfelt, J. phys. Chem. 68 (1964) 2962.
[10] C. Michael, J. Bradford, M.A. Vannice, Appl. Catal. A 142 (1996) 73.
[11] A. Aguinaga, J.C. Delacal, J.M. Asua, M. Montes, Appl. Catal. A 51 (1989) 1.
[12] T.K. Campbell, J.L. Falconer, Appl. Catal. A 50 (1989) 189.
[13] L.B. Schreiber, R.W. Vaughan, J. Catal. 40 (1975) 226.
[14] M.F. Wilson, P.R. Mainwaring, J.R. Brown, J.F. Kriz, Appl. Catal. A 41 (1988) 177.
[15] S. Benbenek, E. Fedorynska, P. Winiarek, React. Kinet. Catal. Lett. 51 (1993) 189.
[16] A. Gil, A. Diaz, L.M. Gandia, M. Montes, Appl. Catal. A 109 (1994) 167.
[17] T.H. Liou, F.W. Chang, Ind. Eng. Chem. Res. 35 (1996) 3375.
[18] T.H. Liou, F.W. Chang, J.J. Lo, Ind. Eng. Chem. Res. 36 (1997) 568.
[19] F.W. Chang, T.J. Hsiao, S.W. Chung, J.J. Lo, Appl. Catal. A 164 (1997) 225.
[20] F.W. Chang, T.J. Hsiao, J.D. Shih, Ind. Eng. Chem. Res. 37 (1998) 3838.
[21] M.T. Tsay, F.W. Chang, Appl. Catal. A 203 (2000) 15.
[22] F.W. Chang, M.T. Tsay, S.P. Liang, Appl. Catal. A 209 (2001) 217.
[23] O. Clause, M. Kermarec, L. Bonneviot, F. Villain, M. Che, J. Am. Chem. Soc. 114 (1992) 4709.
[24] D.G. Mustard, C.H. Bartholomew, J. Catal. 67 (1981) 186.
[25] E.P. Parry, J. Catal. 2 (1963) 371.
[26] J. Medema, J.J.G.M. Van Bokhoven, A.E.T. Kuiper, J. Catal. 25 (1972) 238.

[27] P.S. Kumbhar, Appl. Catal. A 96 (1993) 241.
[28] W. Daniell, U. Schubert, R. Glockler, A. Meyer, K. Noweck, H. Knozinger, Appl. Catal. A 196 (2000) 247.
[29] O. Clause, L. Bonneviot, M. Che, J. Catal. 138 (1992) 195.
[30] M. Kermarec, J.Y. Carriat, P. Burattin, M. Che, A. Decarreau, J. Phys. Chem. 98 (1994) 12008.
[31] B. Scheffer, P. Mdhock, J.A. Moulijn, Appl. Catal. A 46 (1989) 11.
[32] D.C. Puxley, I.J. Kitchener, C. Komodromos, N.D. Perkyns, Preparation of Catalysts, Vol. 3, Elsevier, Amsterdam, 1983, p. 237.
[33] S.C. Ho, T.C. Chou, Ind. Eng. Chem. Res. 34 (1995) 2279.
[34] A.M. Venezia, A. Parmaliana, A. Mezzapica, G. Deganello, J. Catal. 172 (1997) 463.
[35] J. van de Loosdrecht, A.M. van der Kraan, A.J. van Dillen, J.W. Geus, J. Catal. 170 (1997) 217.